AIMS Materials Science, 3(2): 390-403.
DOI: 10.3934/matersci.2016.2.390
Received: 28 January 2016
Accepted: 17 March 2016
Published: 22 March 2016

http://www.aimspress.com/journal/Materials

Research article

Scratch behavior of soft metallic materials

Fabian Pöhl *, Corinna Hardes, and Werner Theisen

Chair of Materials Technology, Ruhr-Universität Bochum, Bochum, Germany

*** Correspondence:** Email: poehl@wtech.rub.de.

Abstract: This paper investigates the scratch resistance of metallic materials that include pure iron and the two steels AISI 1045 and AISI 304L. To investigate the deformation behavior under scratch load, tests were performed with a gradually increasing scratch load combined with subsequent analysis by scanning-electron microscopy and by atomic force microscopy. The f_{ab} value was determined to quantify the active micro-mechanisms of abrasion. In addition, tensile tests, hardness measurements, and nanoindentation experiments were conducted to correlate the scratch behavior with the mechanical properties. It was shown that there is no general correlation between the individual mechanical properties and the results of the scratch tests. However, the results revealed that work hardening of metallic materials plays a significant role, especially in the development of pile-up, and thus it greatly affects the active micro-mechanisms. The specific work of fracture at least correctly reproduces the order of scratch depth and the tangential force of the investigated materials.

Keywords: scratch test; plastic deformation; local deformation behavior; AISI 304L; AISI 1045

1. Introduction

Machine components and tools such as extruders, chutes, and crushers are impaired by abrasive wear [1]. The process of wear involves complex surface interactions and is thus not fully predictable [2]. Even measurement of the wear rate only accounts for the particular tribological system used for the experiment [3]. Nevertheless, the abrasive wear behavior is affected by determinable bulk or surface properties of the contact materials [2]. Hence, further examination of the material behavior under abrasion contributes to an improved understanding of the appearances of abrasive wear. Abrasion can be experimentally reproduced with the help of a single-point scratch test, in which a moving indenter penetrates the surface of the specimen [4]. The scratched surface is

characterized by the active micro-mechanisms of abrasion [5], which are influenced by the deformation behavior of the specimen [1]. The scratch behavior of hard materials and hard coatings is a widely discussed research topic [6,8,9].

This work examines less hard metals such as pure iron, AISI 304L, and AISI 1045. The geometry and extent of the scratches were observed by scanning electron microscopy (SEM) and atomic force microscope (AFM). The mechanical properties of the metals were determined by indentation (macro hardness testing and nanoindentation) as well as tensile testing. The scratch behavior is discussed with respect to the measured mechanical properties. Furthermore, the f_{ab} value, which is often used to quantify the active micro-mechanisms of abrasion, is critically analyzed.

2. Materials and Method

2.1. Examined materials and specimens

The examined materials are pure iron and the steels AISI 1045 and AISI 304L. The chemical composition of AISI 1045 and AISI 304L, measured by spark spectroscopy, is given in Table 1. AISI 1045 was austenitized at 830 °C and slowly cooled to room temperature to achieve a pearlitic-ferritic microstructure, whereas AISI 304L was solution-annealed followed by quenching in water to achieve a homogeneous microstructure and to avoid carbide precipitation.

Table 1. Chemical composition in mass% measured by spark spectroscopy.

Material	C	Si	Mn	P	S	Cr	Ni	Mo	Fe
AISI 1045	0.437	0.245	0.761	0.107	0.032	0.052	0.068	0.014	bal.
AISI 304L	0.021	0.418	1.500	0.040	0.029	18.20	8.500	0.271	bal.

The specimens for scratch and indentation testing were prepared by grinding with SiC paper (1000 mesh) and then successive polishing steps. The final polishing used a diamond suspension with an average grain size of 1 μm. To analyze the microstructure, the specimens were etched. Pure iron and AISI 1045 were etched with a 3 % nitric acid solution and AISI 304L with V2A stain.

2.2. Scratch testing

Scratch tests were conducted with a scratch tester (CSM instruments; NST module) equipped with a sphero-conical diamond (tip radius 10 μm). The test parameters were a gradually increasing load (3 mN to 603 mN) and a scratch speed of 400 μm/min. The applied normal force (P_n) and tangential force (P_t) as well as the resulting scratch depth were continuously measured during the scratch test. Curves of the scratch depth and tangential force as a function of the scratch position were averaged from a minimum of four single scratch tests.

2.3. Indentation testing

The indentation tests were conducted with a Berkovich diamond indenter (CSM instruments; NHT module) with a maximum load of 200 mN, a loading and unloading rate of 400 mN/min, and a dwell time of 10 s at the maximum load. The measured load-displacement curves were evaluated with the traditional OLIVER and PHARR method to determine indentation hardness H_i of the materials [10,11]. Furthermore, the ratio of elastic to total indentation work W_{el}/W_{tot} was calculated from the area under the loading and unloading curve (Figure 1).

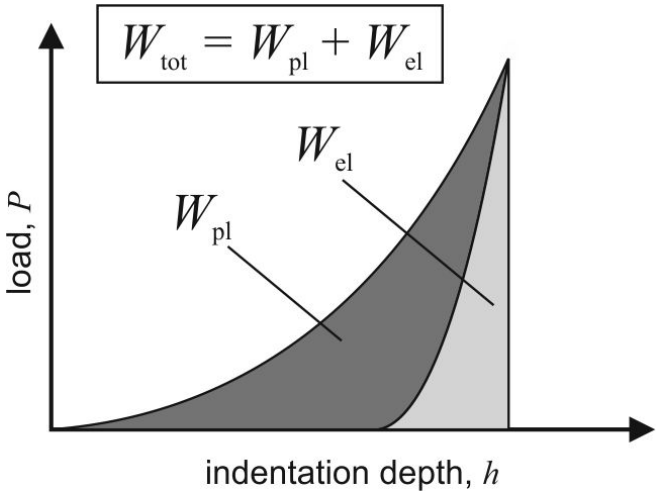

Figure 1. Schematic illustration of the load-displacement curve including the plastic and elastic indentation energies (W_{pl} and W_{el}).

2.4. Scanning electron microscopy and atomic force microscopy

The deformation induced by scratch testing was investigated by scanning electron microscopy (SEM, Tescan Mira) and atomic force microscopy (AFM, Bruker Nanos). The AFM was operated in the contact mode with a scanning speed of 10–40 µm/min. Data evaluation and 3D visualization of the scratches were conducted with the software ImagePlus (Version 2.9). The AFM images enable determination of the f_{ab} value, which is often used to describe the relative fractions of the microabrasion mechanisms of micro-cutting and micro-ploughing [1]. The parameter, given by Eq. (1), relates the area of the groove furrow to the area of the ploughed material beside the groove for a given scratch cross-section (Figure 2).

$$f_{ab} = \frac{A_v - (A_1 + A_2)}{A_v} \tag{1}$$

Assuming purely plastic deformation with consistency of volume, a value of zero corresponds to ideal micro-ploughing with all material being pushed to the sides, whereas a value of one corresponds to ideal micro-cutting with all material being chipped out. The f_{ab} value was determined by evaluating 5 positions along the length of the scratch (Figure 3).

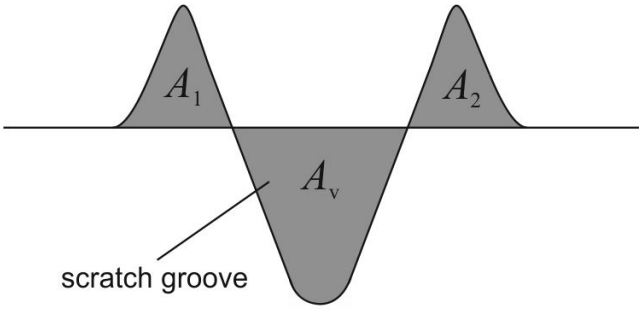

Figure 2. Schematic illustration of a scratch groove (cross-section), including the parameters A_1, A_2, and A_v of the f_{ab} parameter, after ZUM GAHR [1].

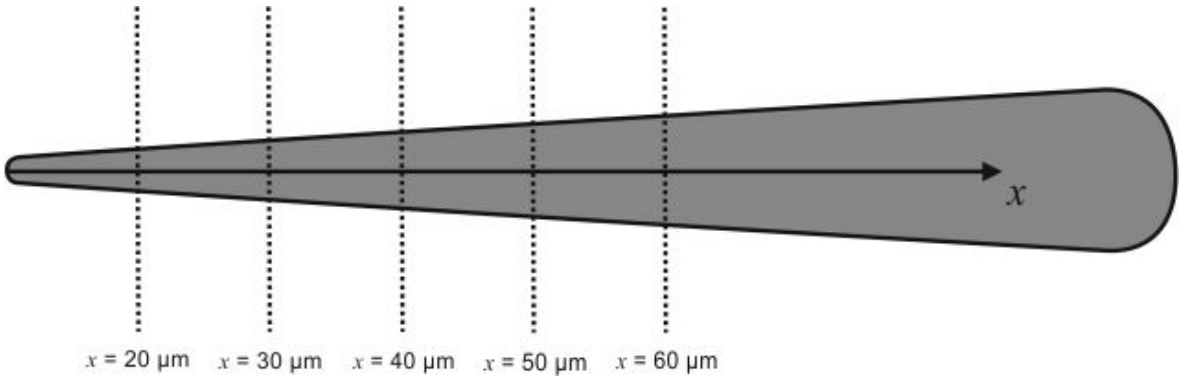

Figure 3. Schematic illustration of the top view of a scratch with gradually increasing load, including the five positions along the length of scratch used for determining the f_{ab} value.

For comparison with the indentation hardness the scratch hardness was calculated for the scratch position of x = 60 µm (see Figure 3). According to Eq. (2) the scratch hardness is defined as the ratio of the normal scratch load P_n to the projected contact area A_p. The projected contact area was calculated for all materials using the cross-sections measured with the AFM at a scratch position of x = 60 µm.

$$HS_P = \frac{2P_n}{A_p} \tag{2}$$

2.5. Tensile testing

Tensile tests were performed using a Z100 machine (Zwick) with quasi-static loading. Curves of the engineering stress/strain and true stress/strain were determined from the measured displacement and force.

3. Results and Discussion

Figure 4 shows the microstructure of the investigated materials. The microstructure of pure iron and the austenitic steel AISI 304L is polycrystalline and single-phase, whereas the steel AISI 1045 consists of two phases – ferrite and pearlite – in the investigated heat treatment condition.

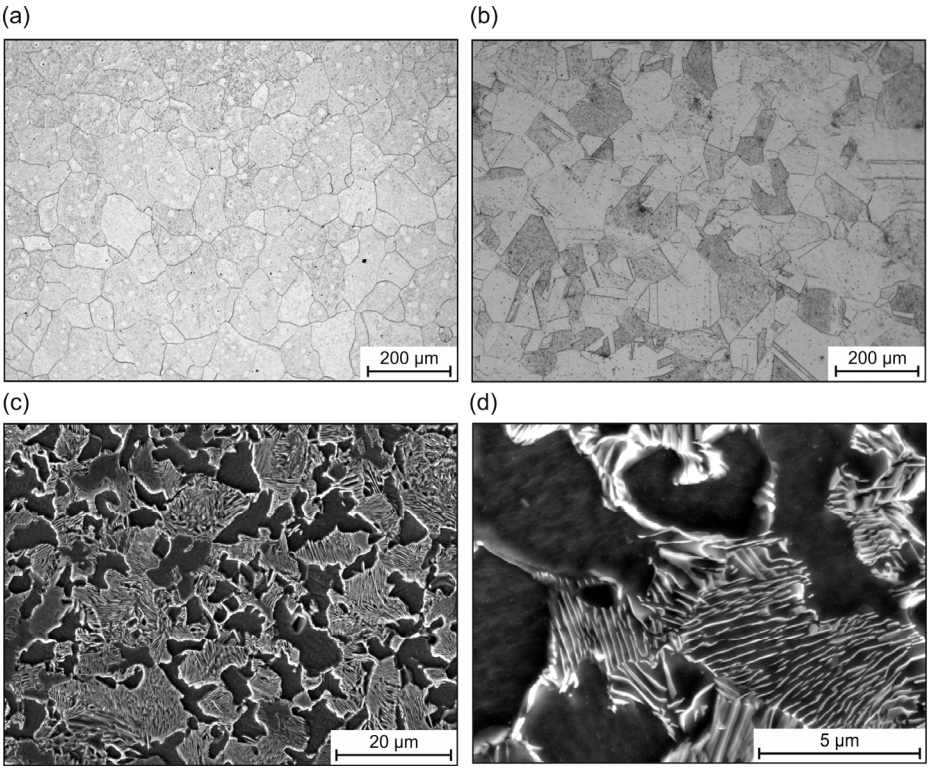

Figure 4. Microstructure of (a) pure iron, (b) AISI 304L, (c) and (d) AISI 1045.

As apparent from Figure 5 the greatest scratch depth was found for pure iron followed by AISI 1045 and AISI 304L. The latter both show a significantly shallower scratch depth. The scratch depth of AISI 304L is only slightly lower than that of AISI 1045. The same tendency holds true for the tangential force. The difference between AISI 1045 and AISI 304L is more evident for the tangential force compared to the scratch depth. A lower scratch depth suggests a greater resistance to abrasion with a reduction in material loss.

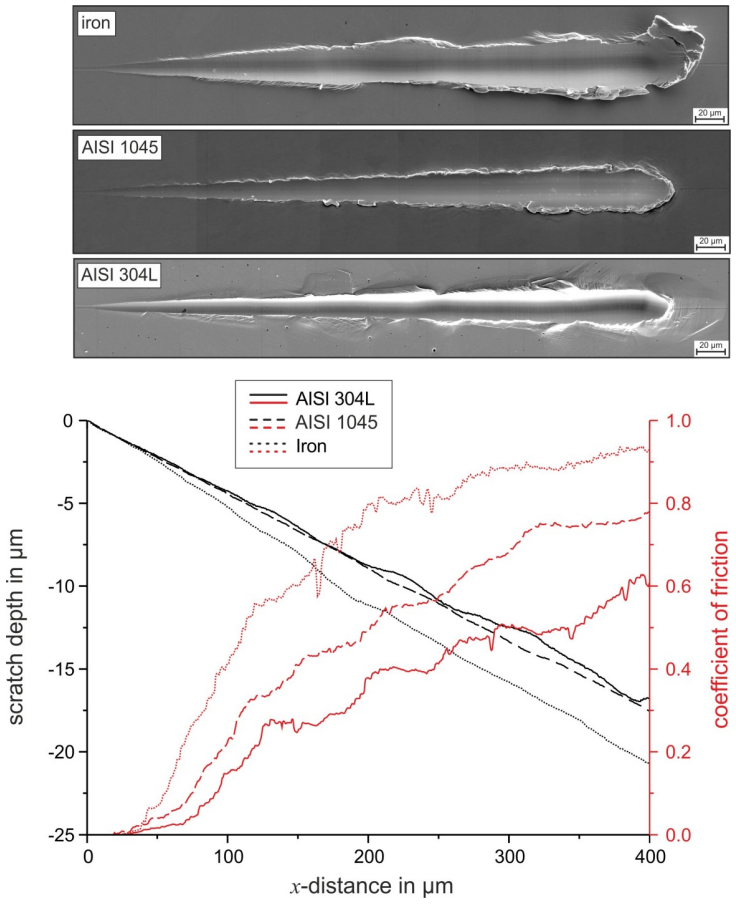

Figure 5. SEM panorama images of the scratch grooves and measured scratch depth as well as coefficient of friction for iron, AISI 1045, and AISI 304L.

Not only the scratch depth but also the deformation behavior, including the micro-mechanisms of abrasion, have a decisive role and define the abrasion resistance. As can be seen in Figs. 6 and 7, scratching of pure iron leads to massive pile-up next to the edges of the scratch. A large volume of scratched material is pushed in front of the indenter and then ploughed to the sides or chipped out. The active micro-mechanisms of abrasion are thus micro-ploughing and micro-cutting.

To quantify the dominating micro-mechanisms, the f_{ab} value was calculated at five positions along the length of the scratch (Figure 3). The mean value of all positions is summarized for the investigated materials in Figure 8. The mean f_{ab} value for pure iron is 0.17 ± 0.21, which suggests that a combination of micro-cutting and micro-ploughing is present in which the fraction of micro-ploughing is larger. From the large standard deviation, it can be concluded that the f_{ab} value strongly varies along the length of the scratch, even for the single-phase pure iron. It is possible that the deformed volume of a longer scratch distance can be ploughed out locally and concentrated at the sides, thus leading to very large pile-ups. In such a case, the f_{ab} value can be zero or even negative. Figure 9 illustrates such deformation behavior. A region of almost no pile-up is followed by a massively concentrated pile-up, which leads to a negative f_{ab} value.

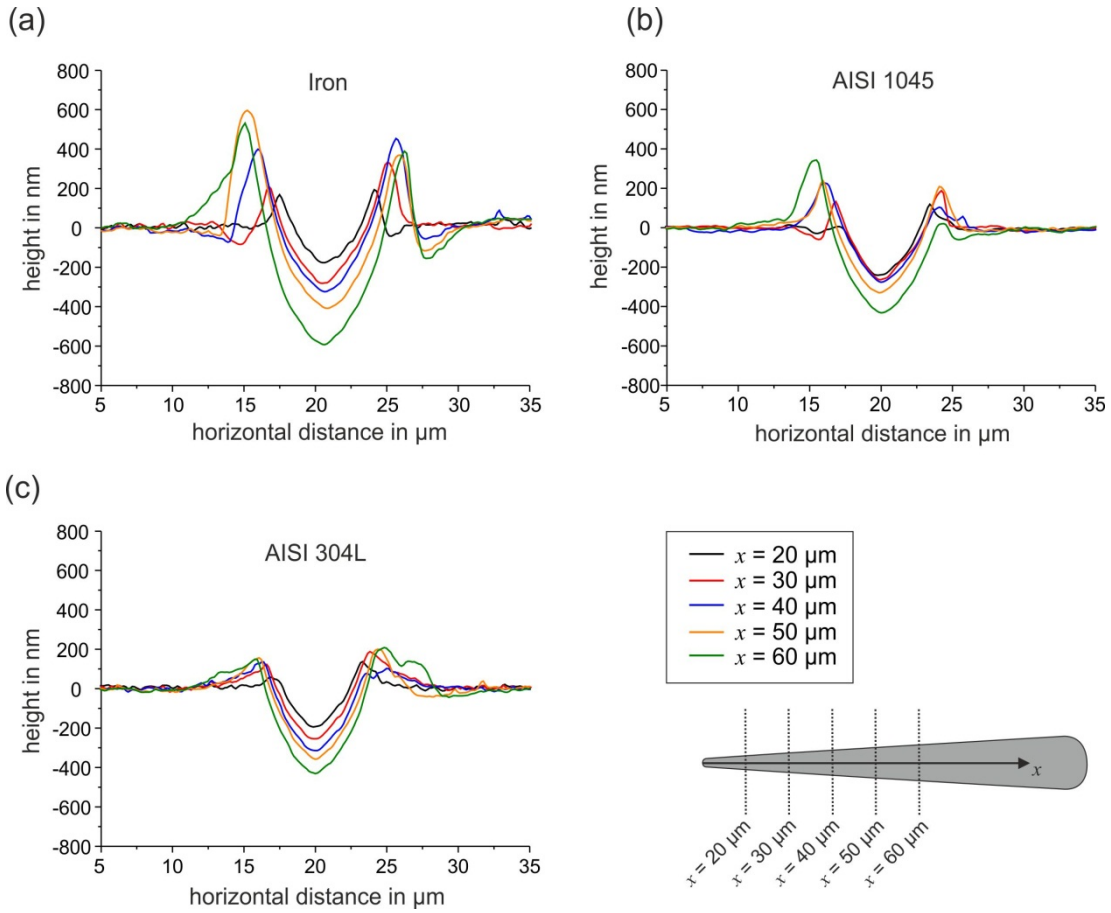

Figure 6. Height profiles at different scratch positions for one individual scratch in (a) pure iron, (b) AISI 1045, and (c) AISI 304L.

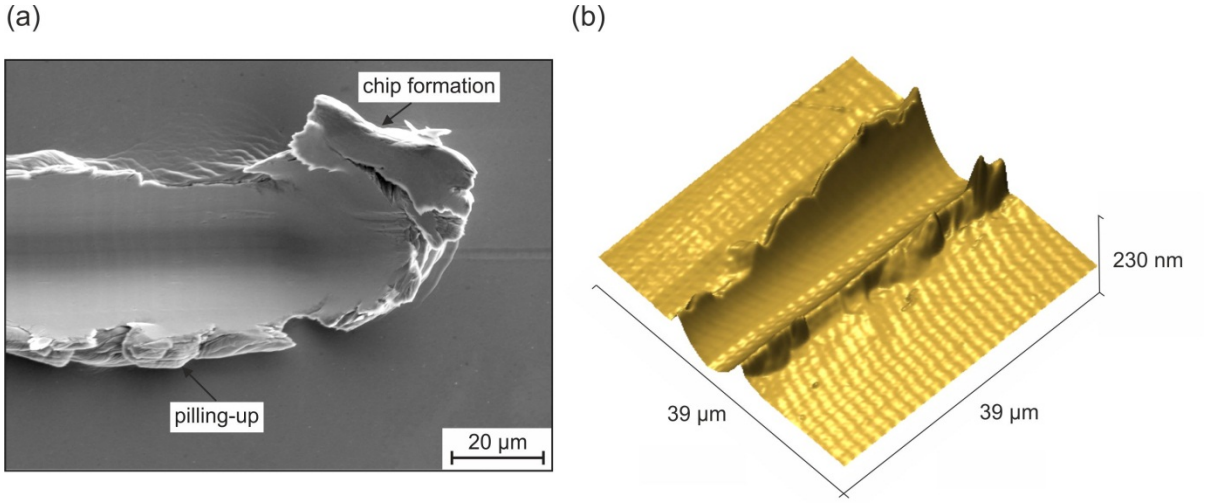

Figure 7. (a) SEM image of a scratch in pure iron with massive pile-up and chip formation (b) AFM topography image of a scratch in pure iron illustrating massive pile-up of the deformed volume next to the scratch groove.

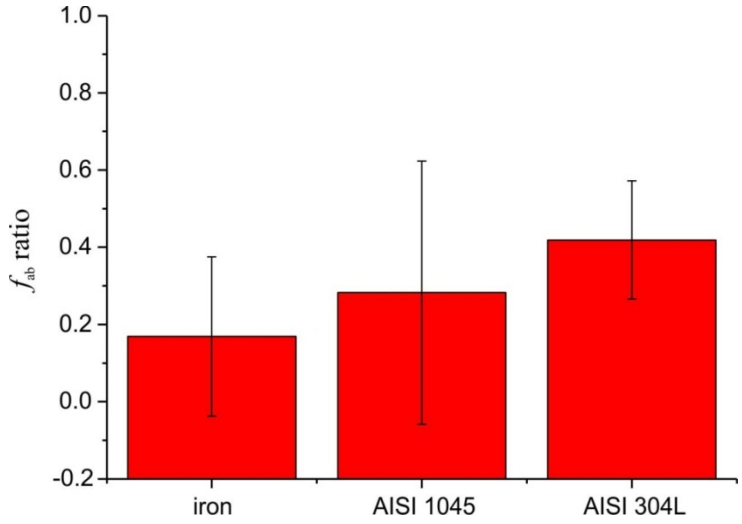

Figure 8. Mean f_{ab} value of the investigated materials.

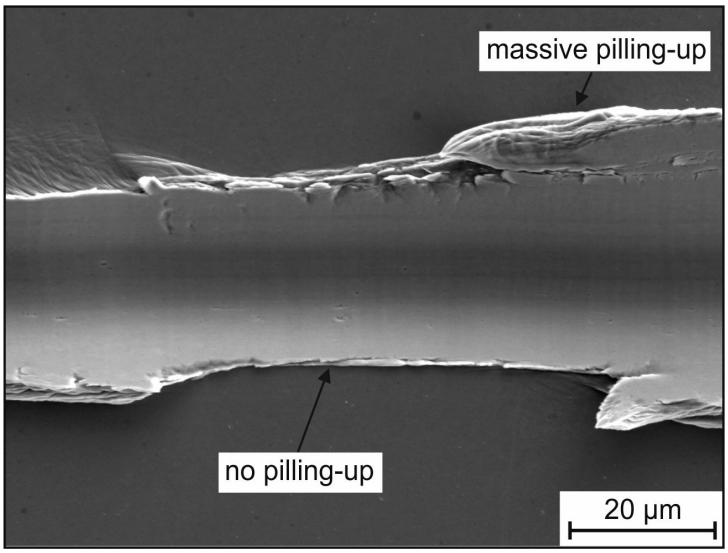

Figure 9. SEM image of a scratch in pure iron showing a region without pile-up followed by a region with massive pile-up.

Figure 10 shows that the crystallographic orientation of the scratched grains also has a very significant effect on the deformation behavior. Depending on the orientation, the imposed stress field leads to activation of dislocation slip. Thus the deformation behavior expressed by the scratch depth, pile-up, and chip formation can differ significantly from one grain to the next. Dislocation slip also causes slip lines with an orientation-dependent pattern on the surface (Figure 10). The matrix of indentations in two different grains in AISI 304L in Figure 11 clearly demonstrates that the local mechanical behavior is dependent on the crystallographic orientation.

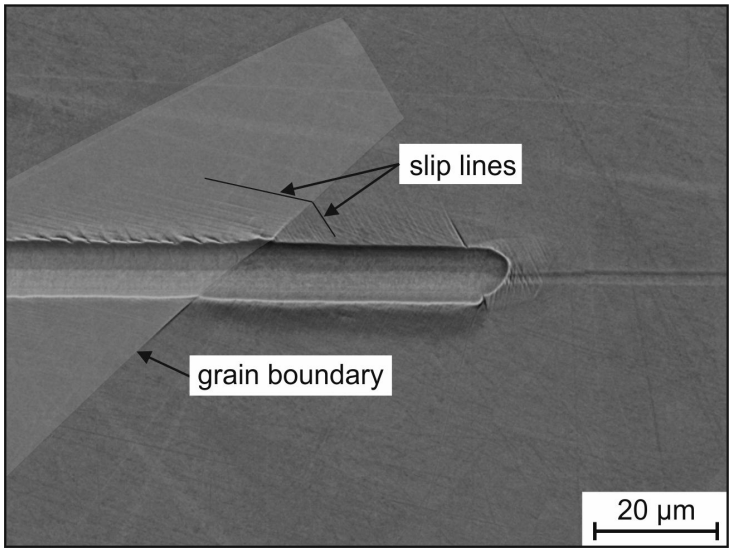

Figure 10. SEM image of a scratch in AISI 304L through different grains.

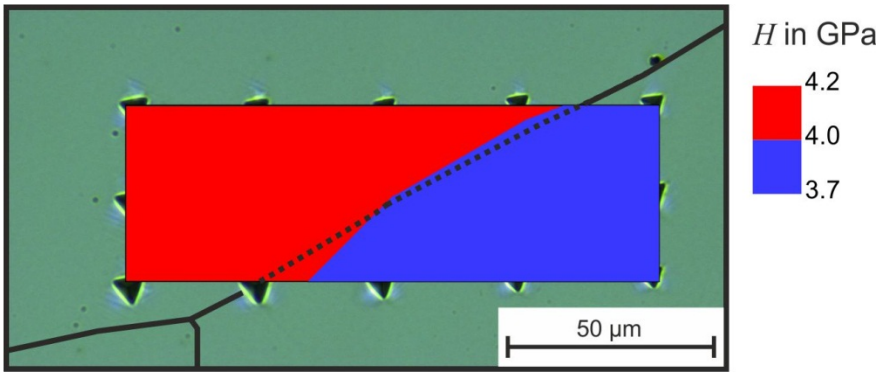

Figure 11. Hardness H of two different grains of AISI 304L measured by a matrix of nanoindentations (the hardness was interpolated between the individual indentations).

Compared to pure iron, the AISI 1045 and AISI 304L steels show a lower pile-up tendency. As Fig 8 proves, pure iron has the lowest f_{ab} value (larger amount of micro-ploughing) followed by AISI 1045 with a large standard deviation and AISI 304L with the lowest f_{ab} value. The large standard deviation of AISI1045 is caused by the two-phase microstructure. Whereas the soft ferrite shows large pile-ups similar to pure iron, the harder pearlite tends to show small pile-ups and a higher f_{ab} value. In conclusion, the pure iron shows a large amount of micro-ploughing with a lot of deformed material pushed to the sides to form large pile-ups. Large pile-ups in combination with a deep scratch depth lead to a high tangential force and thus higher friction coefficient because a large volume of material must be displaced horizontally during scratching. Due to the lower scratch depth and smaller pile-ups, scratching of AISI 1045 and AISI 304L results in lower tangential forces and friction coefficients. The lowest friction coefficient is achieved for AISI 304L, although the scratch depth is only slightly lower compared to AISI 1045. In contrast to AISI 304L, the AISI 1045 shows larger pile-ups (lower f_{ab} value), which leads to a larger volume of horizontally displaced material and thus to a higher tangential force and friction coefficient.

The greatly varying f_{ab} value indicates that it has only a limited suitability for describing the micro-mechanisms of abrasion and strongly depends on the analyzed cross-section. Furthermore, the absence of pile-up does not necessarily imply the presence of micro-cutting, as indicated by the f_{ab} value. An example of such a case is AISI 304L. The mean f_{ab} value (f_{ab} = 0.42) indicates massive micro- cutting, whereas the SEM images (e.g. Figs. 5 and 10) do not show massive chip formation. The discrepancy between the visual results and the f_{ab} value can be explained by elasto-plastic deformation behavior. In contrast to pure iron and AISI 1045, AISI 304L features a high work hardening potential (Figure 12). From indentation testing it is known that the pile-up behavior can be correlated with the work hardening behavior and materials with a high work hardening potential during indentation show a lower pile-up tendency [12,13,14]. In extreme cases, materials can develop sink-in rather than pile-up [15]. BELLEMARE et al. also showed, numerically and experimentally, the strong influence of work hardening on the pile-up behavior for scratching of soft copper and Cu-Zn [16]. Work hardening of surface regions prevents plastic upward flow and thus prevents the formation of distinct pile-up. Since plastic deformation is associated with volume constancy, residual elastic stresses under the scratch groove and under the plastic zone can lead to a f_{ab} value of 0.42 without massive chip formation.

As already described for the formation of pile-up, the deformation behavior under scratch loading is dependent on the mechanical properties of the materials, whereas the scratch resistance is not an intrinsic material property but the response of the multiparameter tribo-system [9]. Figure 12 shows the uniaxial true stress/strain curves of the investigated materials. The tensile curves illustrate that pure iron has a low strength and moderate fracture strain. AISI 304L has a similar yield stress compared to pure iron but a high work hardening potential leading to the highest ultimate tensile strength and highest fracture strain. The steel AISI 1045 shows the highest yield stress with moderate work hardening leading to the lowest fracture strain und an ultimate tensile strength that is higher than that of pure iron and lower than that of AISI 304L. Since the mechanical properties and material parameters such as the yield stress, work hardening behavior, ultimate tensile strength, and fracture strain are linked to the deformation behavior under scratch loading in a complex manner, it is not possible to directly correlate them to the measured scratch depth, tangential force, friction coefficient, or f_{ab} value.

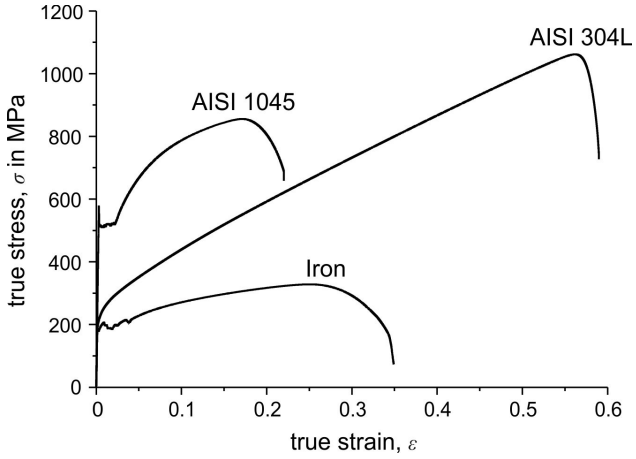

Figure 12. True stress/strain curves of the investigated materials.

It can be concluded that the low strength of pure iron leads to the greatest scratch depth and that the low work hardening potential leads to the formation of massive pile-up. As a consequence, a combination of micro-ploughing and a significant amount of micro-cutting occurs. The large scratch depth and large pile-up formation result in a high tangential force and high friction coefficient. In contrast, the higher strength of AISI 1045 and the greater work hardening behavior lead to a lower scratch depth and a lower amount of pile-up. The tangential force and friction coefficient is thus decreased compared to pure iron. In the case of AISI 1045, the scratch depth and tangential force are the result of the compound behavior of the two-phase microstructure, which consists of pearlite and ferrite. As shown in Figure 13, the deformation of soft ferrite corresponds more closely to pure iron with greater pile-ups. The deformation of pearlite with a higher strength leads to a local reduction in scratch depth with smaller pile-up volume. This holds true as long as the scratch width is smaller than the size of the single phases. For greater scratch depths, the deformation behavior is the compound behavior of both phases. Compared to AISI 304L, the steel AISI 1045 shows a similar scratch depth, which is the result of the compound behavior with a higher yield stress but a lower ultimate tensile strength and lower fracture strain. The lower work hardening potential of AISI 1045 leads to a larger pile-up and thus to a significantly higher tangential force and friction coefficient, although the scratch depth is only slightly higher than that of AISI 304L.

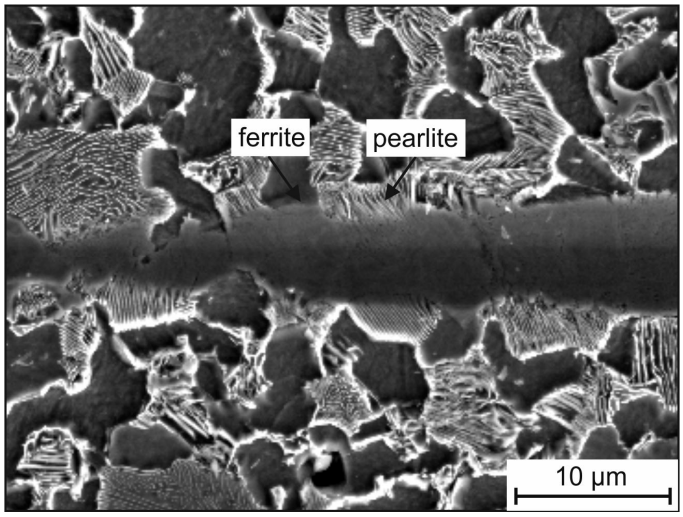

Figure 13. SEM image of a scratch showing the deformation behavior of ferrite and pearlite.

As in the case with the properties derived from the tensile test, the Vickers macro hardness, indentation hardness measured by nanoindentation, scratch hardness, as well as the ratio of elastic to total indentation work also do not correlate with the scratch depth or friction coefficient. The measured parameters are summarized in Table 2. Although AISI 1045 has a greater hardness and a higher W_{el}/W_{tot} ratio than AISI 304L, the scratch depth of AISI 1045 is slightly higher and its friction coefficient is considerably higher. This demonstrates not only the complexity of scratch-induced deformation with the included difficulty of finding correlations, but also the strong influence of the work hardening behavior. In conclusion, the scratch behavior of metallic materials is governed by a combination of different material parameters. Since the hardness does not significantly account for strain hardening (mean induced strain of a Vickers and Berkovich indenter is approx. 8 % [17]), it is not possible to use this parameter to predict the scratch behavior or in general for predicting the

deformation behavior under abrasion. Single mechanical parameters of the tensile curve also do not show correlations to the scratch behavior. One possible way of combining the different mechanical properties of the tensile test is the specific work of fracture, which is the area under the stress/strain curve. As can be seen in Figure 14, there is a reasonable correlation between the specific work of fracture and the scratch depth as well as the friction coefficient. At least the order of the three materials is correctly reproduced.

Table 2. Mechanical properties measured by indentation and scratch testing.

Material	Vickers hardness in HV10	Indentation hardness H in GPa	W_{el}/W_{tot} in %	Scratch hardness HS_P in GPa (for x = 60 µm)
Iron	80 ± 3	1.58 ± 0.04	5.6 ± 0.4	1.90
AISI 1045	209 ± 1	2.01 ± 0.03	10.4 ± 0.5	3.21
AISI 304L	131 ± 1	1.75 ± 0.05	7.4 ± 0.8	2.99

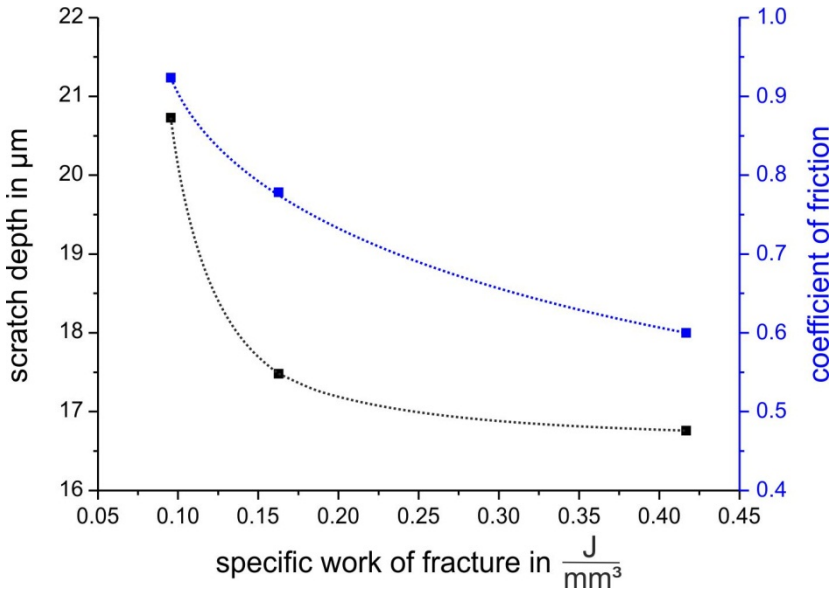

Figure 14. Scratch depth and friction coefficient as a function of the specific work of fracture.

Future work could address a more detailed optical 3D analysis of scratches by e.g. interferometry. Among the fab value and mechanical parameters presented here further topology parameters of the scratches could be considered to find further correlations to the abrasive wear behavior [18,19]. Additionally, numerically-assisted (Finite-Element-Method) analysis of scratching can be considered to determine the mechanical behavior including the induced stresses and strains in the material [20].

4. Conclusion

This study investigated the scratch behavior of metallic materials. The following conclusions can be drawn:

- Iron has the lowest scratch resistance with the largest scratch depth and highest tangential force and friction coefficient. Although the f_{ab} value suggests micro-ploughing is the dominant micro-mechanism, the SEM analysis of the scratches revealed that significant micro-cutting occurred.
- The deformation behavior of iron is governed by massive pile-ups at the sides of the scratch that, in combination with the large scratch depth, explains the large tangential force and friction coefficients. From the large standard deviation, it can be concluded that the f_{ab} value greatly varies along the length of the scratch. The deformed volume of a longer scratch distance can be ploughed out locally and concentrated at the sides leading to very large local pile-ups.
- The large scratch depth and large pile-ups are caused by the low strength and low work hardening potential of pure iron.
- Compared to pure iron, the scratch resistance of AISI 1045 and AISI 304L is higher. Both have a similar scratch depth, although AISI 1045 has a significantly higher tangential force and friction coefficient.
- The f_{ab} value suggests greater amounts of micro-cutting for AISI 1045 and AISI 304L, whereas the visual analysis revealed that almost no micro-cutting occurred, especially in the case of AISI 304L. This discrepancy can be explained by the greater work hardening ability of the materials. High work hardening can prevent the formation of massive pile-up, very similar to indentation testing.
- For the investigated materials, the f_{ab} value has only a very limited suitability for describing the micro-mechanisms.
- It is not possible to correlate individual mechanical properties such as the hardness or yield stress to the scratch depth and friction coefficient. Thus the scratch behavior and deformation behavior under abrasion cannot be predicted on the basis of individual mechanical properties. In contrast, is a combination of different material parameters govern the scratch behavior of metallic materials. One possible way of combining the different mechanical properties of the tensile test is the specific work of fracture, which does at least correctly reproduce the order of scratch depth and friction coefficient in the investigated materials.

Conflict of Interest

The authors declare no competing financial interest.

References

1. Zum Gahr K-H (1987) Microstructure and wear of materials, Elsevier.
2. Rabinowicz E (1965) Friction and wear of materials, John Wiley and Sons.
3. Fischer A (1988) Sliding wear of metallic materials at 25 and 550°C, Materials Research Society, Fall meeting.
4. Berns H, Fischer A, Kleff J (1993) Scratch tests on iron-, nickel- and cobalt-based alloys at elevated temperatures. *Wear* 162–164: 585–589.

5. Kayaba T, Hokkirigawa K, Kato K (1986) Analysis of the abrasive wear mechanism by successive observations of wear processes in a scanning electron microscope. *Wear* 110: 419–430.
6. Perry A-J (1983) Scratch adhesion testing of hard coatings. *Thin Solid Films* 107: 167–180.
7. Buckley D-H, Rabinowicz (1986) Fundamentals of the wear of hard materials. 2nd International Conference Science Hard Materials, Rhodes.
8. Rodrigo A (2001) Analytical correlation of hardness and scratch adhesion for hard films. *Surf Coat Tech* 148: 8–17.
9. Xu X, Van der Zwaag S, Xu W (2016) The effect of martensite volume fraction on the scratch and abrasion resistance of a ferrite-martensite dual phase steel. *Wear* 348–349: 80–88.
10. Oliver W-C, Pharr G-M (1992) An improved technique for determining hardness and elastic modulus using load and displacement sensing indentation experiments. *J Mater Res* 7: 1564–1583.
11. Oliver W-C, Pharr G-M (2003) Measurement of hardness and elastic modulus by instrumented indentation: Advances in understanding and refinements to methodology. *J Mater Res* 19: 3–20.
12. Biwa S, Storakers B (1995) An analysis of fully plastic Brinell indentation. *J Mech Phys Solids* 43: 1303–1333.
13. Field J-S, Swain M-V (1995) Determining the mechanical properties of small volumes of materials from submicron spherical indentations. *J Mater Res* 10: 101–112.
14. Pöhl F, Huth S, Theisen W (2014) Indentation of self-similar indenters: An FEM-assisted energy-based analysis. *J Mech Phys Solids* 66: 32–41.
15. Lee J-M, Lee C-J, Lee K-H, et al. (2012) Effects of elastic-plastic properties of materials on residual indentation impressions in nano-indentation using sharp indenter. *T Nonferr Metal Soc* 22: 585–595.
16. Bellemare S-C, Dao M, Suresh S (2008) Effects of mechanical properties and surface friction on elasto-plastic sliding contact. *Mech Mater* 40: 206–219.
17. Fischer-Cripps A-C (2002) Nanoindentation, Springer.
18. Kobrick R-L, Klaus D-M, Street Jr KW (2011) Validation of proposed metrics for two-body abrasion scratch test analysis standards. *Wear* 270: 11–12, 815–822.
19. Kobrick R-L, Klaus D-M, Street Jr K-W (2011) Standardization of a volumetric displacement measurement for two-body abrasion scratch test data analysis. *Wear* 270: 9–10, 650–657.
20. Pöhl F, Schwarz S, Junker P, et al. (2015) Indentation and Scratch Testing-Experiment and Simulation. Proceedings of the 3rd International Conference on Stone and Concrete Machining (ICSCM), 319–336.

AIMS Press